ANALYSIS OF THE DISCRETE REPRESENTATION METHOD TO COMPUTE ECHO RESPONSES FROM CIRCULAR CONCAVITY DEFECT

Paulo Orestes Formigoni, paulo.formigoni@poli.usp.br
Orlando Cirullo Filho, cirullinux@gmail.com
School of Engineering at University of São Paulo, Department of Mechatronics Engineering
Av. Prof. Mello Moraes, 2231, CEP 05508-900, São Paulo, Brazil
Julio C. Adamowski, jcadamow@usp.br
School of Engineering at University of São Paulo, Department of Mechatronics Engineering
Av. Prof. Mello Moraes, 2231, CEP 05508-900, São Paulo, Brazil
Flávio Buiochi, fbuiochi@usp.br
School of Engineering at University of São Paulo, Department of Mechatronics Engineering
Av. Prof. Mello Moraes, 2231, CEP 05508-900, São Paulo, Brazil

Abstract. *This works analyzes the discrete representation method to compute the acoustic wave generated by ultrasonic transducers, its interaction with a concave circular defect on a plane surface, and the echoes received by the transducer. The method is divided into three computational parts. As first step, the velocity potential impulse response is determined at the interface using the Rayleigh integral. In a second step, the reflected field is calculated considering that every elementary portion of the interface radiates a hemispherical wave (Huygens principle). Finally, the acoustic pressure over the surface of the receiver is determined by a temporal convolution between the excitation signal and the spatial reflected velocity potential impulse response. The accuracy and the temporal cost of computations depend on the spatial sampling of the aperture and interface, and on the time sampling of the transmitted signals. The aim of the work is to determine a compromise between the accuracy and the computation time, having the temporal sampling of the transmitted signal and the spatial sampling of the aperture and interface with the defect as variables.*
***Keywords** Acoustic field, ultrasound, simulation, impulsive response, pulse-echo response*

1. INTRODUCTION

The investigation of the echo responses caused by circular type defects is an important tool for nondestructive testing using broadband ultrasonic transducer. For instance, the preventive maintenance of pipelines requires finding pitting corrosion defects, which can be done by using pulse-eco mode. It tries to get as much information as possible from the existing defect. However, identifying the defect geometry is not an easy task in realistic situation. Modeling of echo responses from circular concavity defects allows both recognizing the variability of echoes as corrosion grows and selecting the optimal broadband ultrasonic transducer, such that the axial and lateral resolutions are improved. In this work the discrete representation method is described.

The discrete representation method is a computational method that predicts the echo response of arbitrary geometry of defects, using a model that calculates the longitudinal wave evolution caused by interfaces [3], based on the impulse response method [1] and the discrete representation method [4], [5]. This method is suitable for all field regions and can be performed for any excitation wavelength.

The validation of the wave propagation models implemented in the ongoing paper requires experimental corroboration, which is done by using broadband ultrasonic transducers operating in pulse-echo mode and a circular concavity defect embedded in planar reflector. A 19-mm-diam 2.25-MHz transducer and a 6.3-mm-diam, a 10-mm-diam, and 19-mm-diam 5-MHz transducer were used. The errors between experimental and theoretical curves were analyzed by varying the aperture and the reflector surface discretization and the processing times were studied.

2. DISCRETE REPRESENTATION METHOD

The computational method solution proposed by Buiochi et al. [3], which calculates the acoustic field through interfaces, is easily used to calculate the pulse-echo responses using the same theoretical concepts. The proposed solution is an approximated method that operates by dividing the aperture and the interface with a defect into elementary areas, as shown in Fig. 3. The radiated and reflected acoustic fields result from the superposition of the hemispherical waves generated, respectively [6,7,8], from each emitter and interface elementary areas. In this work, as the defect is slightly concave, and the emitter/receiver aperture and the planar interface are parallels, the mode conversion at the reflector surfaces was not considered.
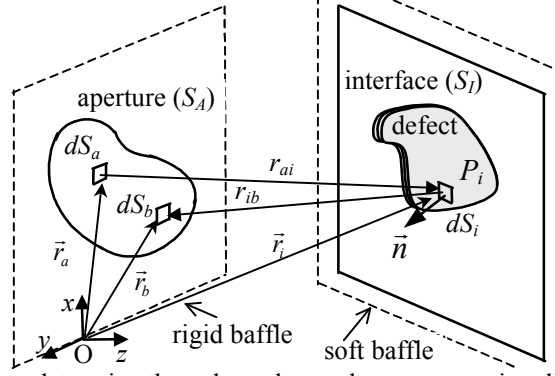
Fig.3. Arbitrary geometry used to determine the pulse-echo mode response using discrete representation method.

Considering an aperture with arbitrary radiating surface S_A embedded in an infinite rigid baffle, the velocity potential impulse response on each point P_i at the interface due to the aperture radiation is given by:

$$h^I(\vec{r}_i,t) = \int_{S_A} \frac{\delta(t - r_{ai}/c)}{2\pi r_{ai}} dS_a \qquad (7)$$

where r_{ai} is the distance from each radiating elementary area dS_a to the point P_i.

Assume that the interface with defect is embedded in an infinite soft baffle and that it is large enough to intercept the main incident energy of the acoustic beam. The whole-extended interface and the defect are approximated by elementary areas dS_i. In each of the receptor aperture elementary areas dS_b, the velocity potential impulse response is calculated from the impulse response obtained at the interface by:

$$h^A(\vec{r}_b,t) = \frac{1}{2\pi c} \int_{S_I} \frac{\cos\theta_{ib}}{r_{ib}} \frac{\partial}{\partial t} h^I(\vec{r}_i, t - \frac{r_{ib}}{c}) dS_i \qquad (8)$$

where S_I is the surface of the interface with the defect, r_{ib} is the distance from the elementary area dS_i located at $\vec{r}_i$ to the point located at $\vec{r}_b$ in the aperture, and θ_{ib} is the angle between the normal vector at P_i and the vector $\vec{r}_{ib}$.

Finally, the spatial acoustic pressure $\langle p(\vec{r}_b,t) \rangle$ over the surface of the finite receiver is calculated by the following temporal convolution:

$$\langle p(\vec{r}_b,t) \rangle = \rho \frac{\partial v(t)}{\partial t} * \langle h(\vec{r}_b,t) \rangle \qquad (9)$$

where $v(t)$ is the excitation signal, ρ is the density of the propagation medium, and $\langle h(\vec{r}_b,t) \rangle$ is defined by:

$$\langle h(\vec{r}_b,t) \rangle = \int_{S_A} h^A(\vec{r}_b,t) dS_b \qquad (10)$$

Thus, it can predict in a rather realistic way, the impulse ultrasonic field generated by a transducer into a part during a non-destructive testing operation in immersion [9-10].

3. RESULTS

Echo responses were obtained from a circular concavity defect to test the validity of the discrete representation method. Fig. 4 shows the geometry of such defect, which was produced on the plane surface of an aluminum solid sample. It also shows the seven positions used to simulate the transducers displacements. Setting the center of the defect as zero (position 1), the positions 1 through 7 are displaced x_{off} = 0, 5, 10, 15, 20, 25 and 30 mm, respectively. The transducers were placed 10 mm from the plane surface of the sample and were excited with short pulses by a pulser/receiver Panametrics 5072PR, Oscilloscope DSO6052-A of 500MHz (Agilent Technologies). All measurements were carried out in water (ρ=1000 kg/m^3, c=1480 m/s), using four transducers: 19-mm-diam 2.25-MHz transducer 25MHz (*V305-512968, Panametrics, USA*), 6.3-mm-diam 5-MHz transducer (*0043V3 alpha, Aeroteck, USA*), a 10-mm-diam 5-MHz transducer (*USP-EPUSP, Brazil*), and 19-mm-diam 5-MHz transducer (*008700 alpha, Aeroteck, USA*).

Simulations were performed in Matlab using the same parameters described above for the experiments in order to allow the comparison of echo responses arising from the defect. The excitation signals used in the simulations were acquired by a 0.6-mm-diameter needle hydrophone placed approximately 3 mm from the transducer faces, considering only the plane waves. For the discrete representation method, the emitter aperture, the interface with the defect, and the receiver aperture discretizations ($\Delta x = \Delta y$) were, respectively, 0.15 mm, 0.2 mm, and 0.2. For all cases, the sampling period was 16 ns.
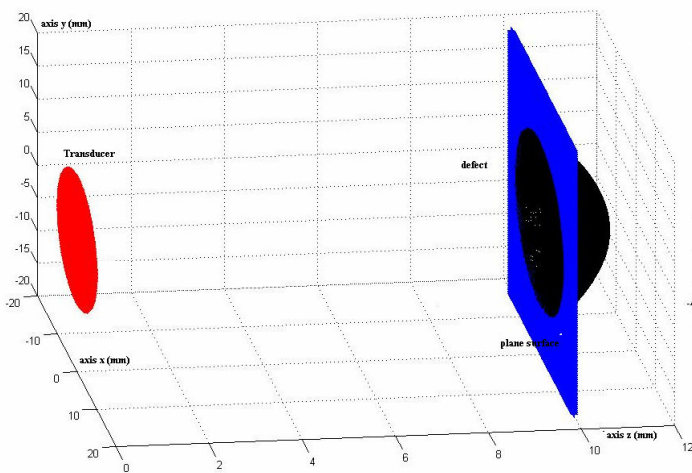
To give an indication of the approach accuracy, the error respect to the experimental echo response has been calculated for every simulated echo signal in the time domain as:

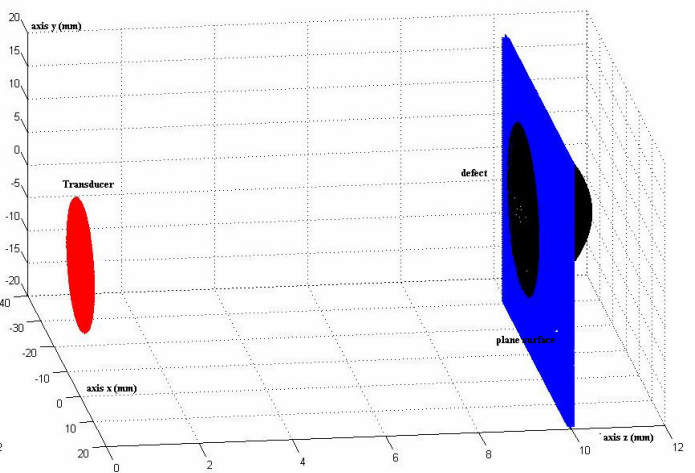$$e = \sqrt{\frac{1}{N} \sum_{i=1}^{N} \left(s_E(i) - s_C(i) \right)^2} \tag{11}$$

where $s_E(i)$ is the experimental signal, $s_C(i)$ is the signal computed by the discrete representation method and N the number of samples.
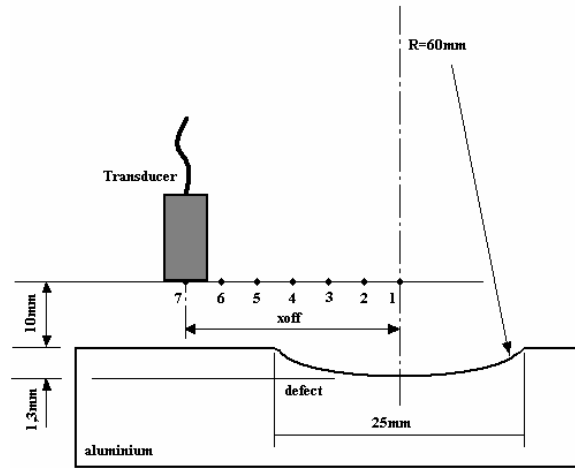

Fig.4. Experimental geometry. (a) Positions 1, 2, 3, 4, 5, 6 and 7 represent, respectively, the transducers displaced 0, 5, 10, 15, 20, 25 and 30 mm from the defect axis; (b) position 7 represented by the 3D model; (c) position 4 represented by the 3D model.

The theoretical and experimental results shown in Fig. 5 until 9 were obtained from a 5-MHz transducer with diameter 6.3 mm at positions 7, 4, 3, 2 and 1, respectively. All signals were normalized by the maximum simulated and experimental amplitudes obtained at position 7. For this transducer, the relative errors between the experimental and theoretical echo responses for positions 1, 2, 3, 4 and 7 are, respectively, 12.6%, 3.8%, 1.4%, 11.1% and 16.0%.
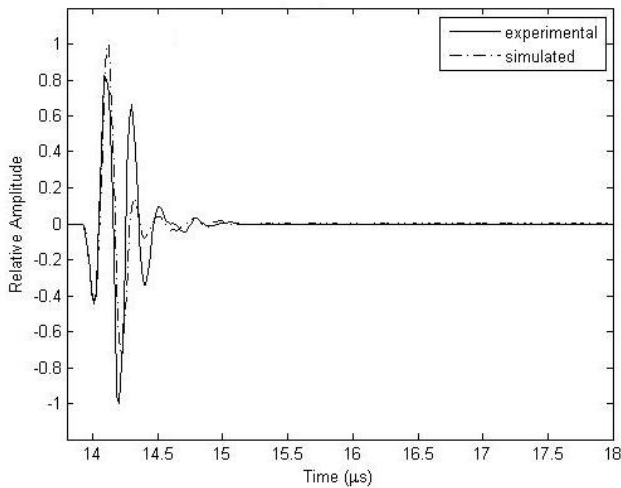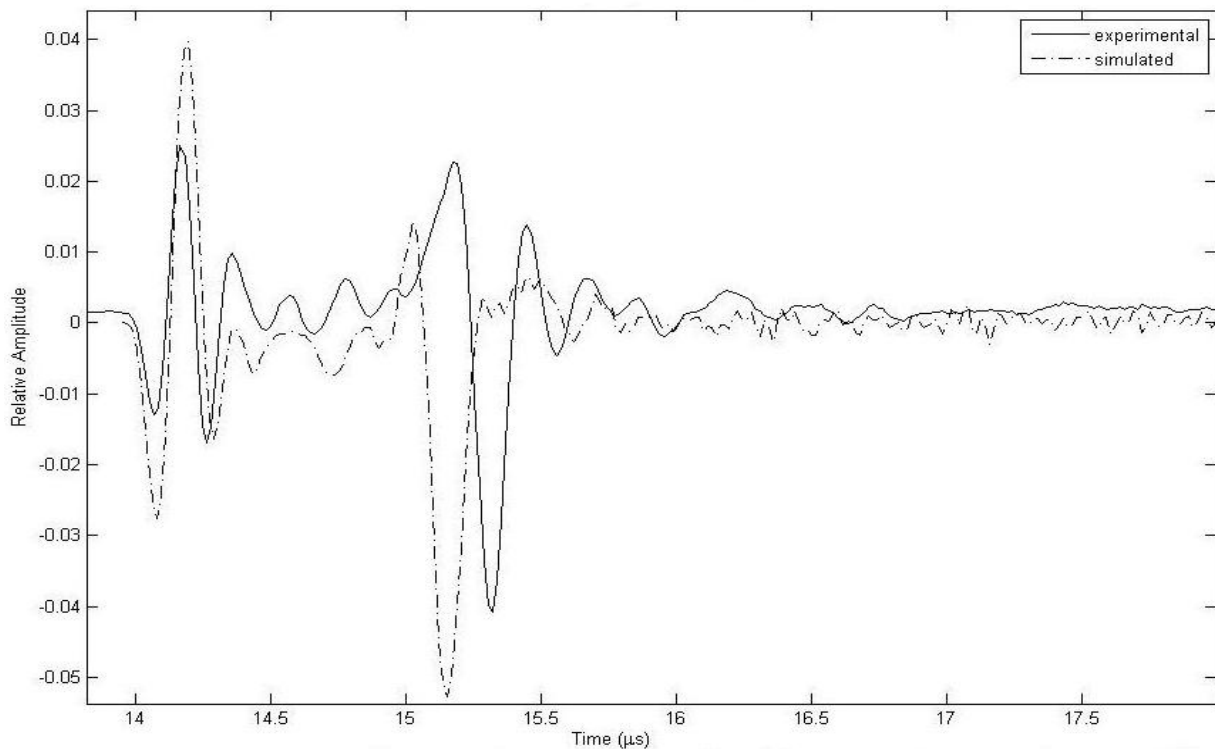
Fig.5. Discrete representation method impulse response (dash-dotted line) and experimental (solid line) signals obtained by using the 5-MHz transducer displaced off the defect axis: (Position 7) 30mm.
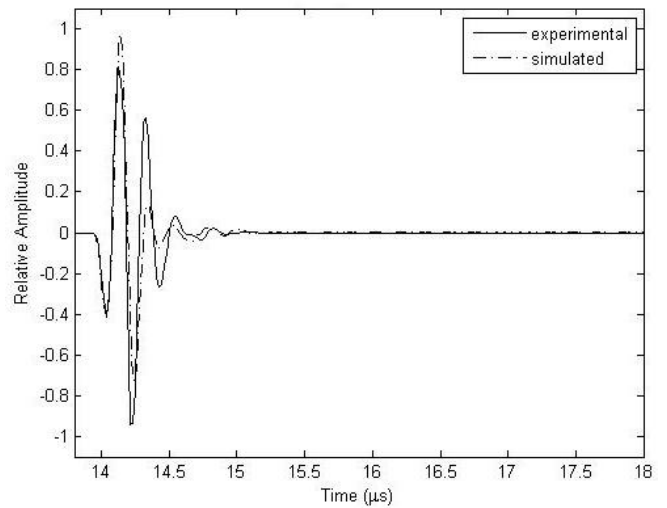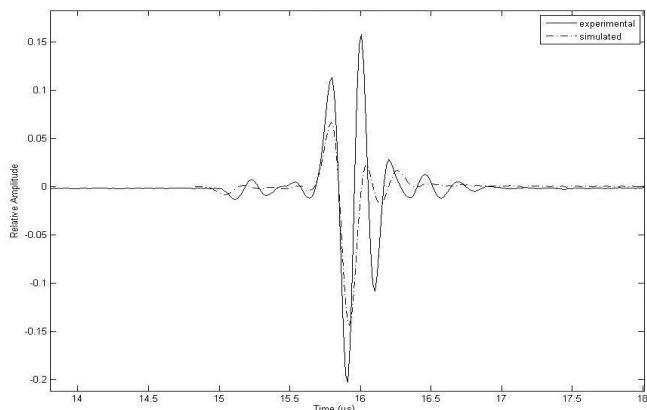
Fig.6. Discrete representation method impulse response (dash-dotted line) and experimental (solid line) signals obtained by using the 5-MHz transducer displaced off the defect axis: (Position 4) 15mm.

Fig.7. Discrete representation method impulse response (dash-dotted line) and experimental (solid line) signals obtained by using the 5-MHz transducer displaced off the defect axis: (Position 3) 10mm.
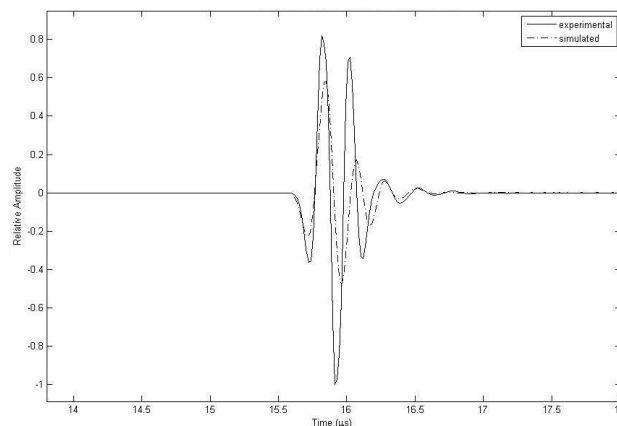
Fig.8. Discrete representation method impulse response (dash-dotted line) and experimental (solid line) signals obtained by using the 5-MHz transducer displaced off the defect axis: (Position 2) 5mm.
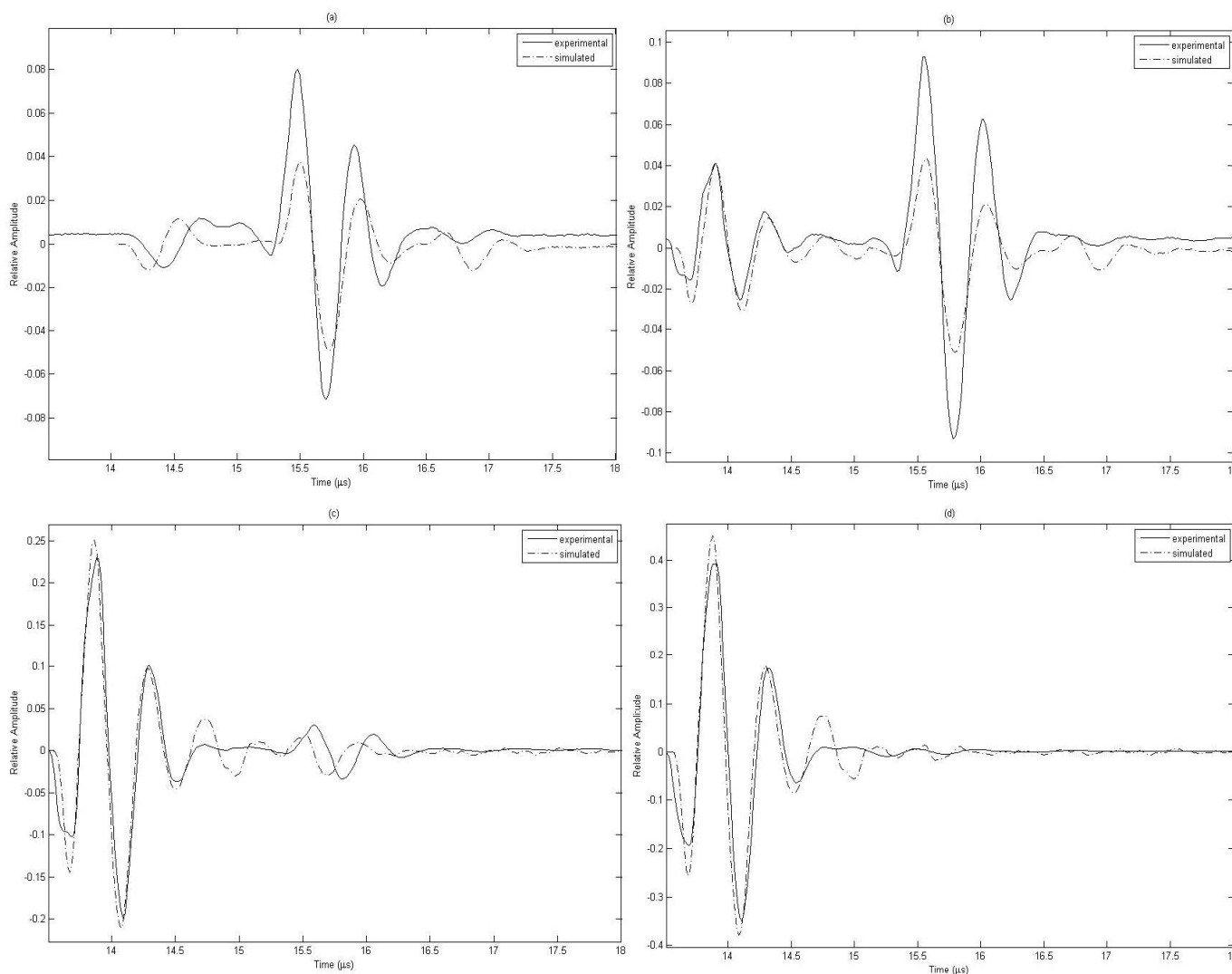

Fig.9. Discrete representation method impulse response (dash-dotted line) and experimental (solid line) signals obtained by using the 5-MHz transducer displaced on the defect axis: (Position 1) 0 mm.

Figure 10 shows the transducer of 2.25 MHz, with 19 mm in diameter in 4 positions, respectively. All signals were normalized by the maximum simulated and experimental amplitudes using the respective transducer at position 7. (a) position 1 = 0mm, (b) position 2 = 5mm, (c) position 3 = 10mm and (d) position 4 = 15mm displaced in axis of defect.

The experimental and simulated values are equal in positions 4, 5, 6 and 7, so no need to show graphs 5, 6 and 7. The same happens in Figure 11 with the transducer made in USP with frequency of 5MHz and 10mm in diameter.

Fig.10. Discrete representation method impulse response (dash-dotted lines) and experimental (solid lines) signals obtained by using the 2.25-MHz transducer, diameter 19mm, displaced off the defect axis: (a) position 1 = 0mm, (b) position 2 = 5mm, (c) position 3 = 10mm, and (d) position 4 = 15mm.

The RMS (Root Mean Square) in 2.25-MHz transducer with 19mm is 18.7720% for position 1, 3.7904% for position 2, 1.3647% for position 3, 11.0630% for position 4. For instance, using a 2.4-GHz Intel Core 2 Duo computer, the processing time for the discrete representation method takes some hours (2-12h) varies with the chosen discretization. The table 1 shows for times for the 4 positions, for 4 transducers used, and also in table 2 shows the times for Δx of 0.4 to 3.0mm respectively, but was simulated from 0.09 until 4.5mm

Table 1: Time of Simulation for each transducer in positions 1 to 4.

Frequency Transducer	Diameter	Times (minutes)			
		Position 1	Position 2	Position 3	Position 4
2.25MHz	19mm	145.13	210.37	264.42	317.66
5MHz	19mm	142.53	202.63	313.12	331.54
5MHz	10mm	32.94	44.17	53.00	72.42
5MHz	6.3mm	13.77	15.92	26.38	34.27

**Table 2:** Time of Simulation for *Δx*; the smaller the size of *Δx* the largest discretization

Frequency Transducer	Diameter	Δx (mm) and Time (minute)			
		0.4mm	0.6mm	0.8mm	1.0mm
2.25MHz	19mm	34.00 min	14.50 min	9.03 min	5.93 min
5MHz	19mm	35.52 min	15.56 min	9.58 min	6.47 min
5MHz	10mm	8.43 min	3.80 min	2.67 min	1.56 min
5MHz	6.3mm	3.56 min	1.63 min	1.03 min	0.69 min
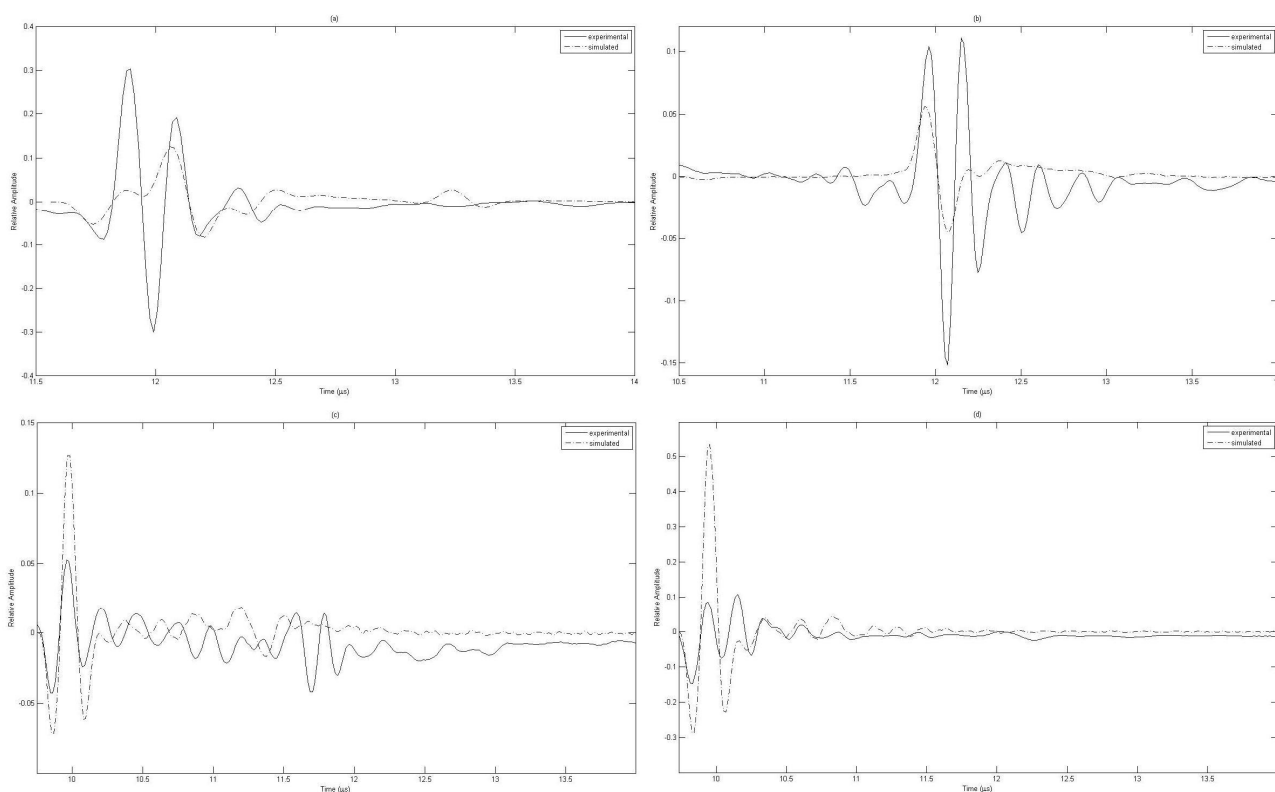
Fig.11. Discrete representation method impulse response (dash-dot line) and experimental (solid lines) signals obtained by using the 5-MHz transducer made USP with diameter 10mm, displaced off the defect axis: (a) position 1 = 0mm, (b) position 2 = 5mm, (c) position 3 = 10mm, and (d) position 4 = 15mm.

The RMS (Root Mean Square) in 5-MHz transducer with 10mm is 7.3947% for position 1, 2.9962% for position 2, 2.3685% for position 3, 7.5568% for position 4. In the 5-MHz transducer with 19mm is 2.6662% for position 1, 3.6123% for position 2, 12.8926% for position 12.5327% for position 4.
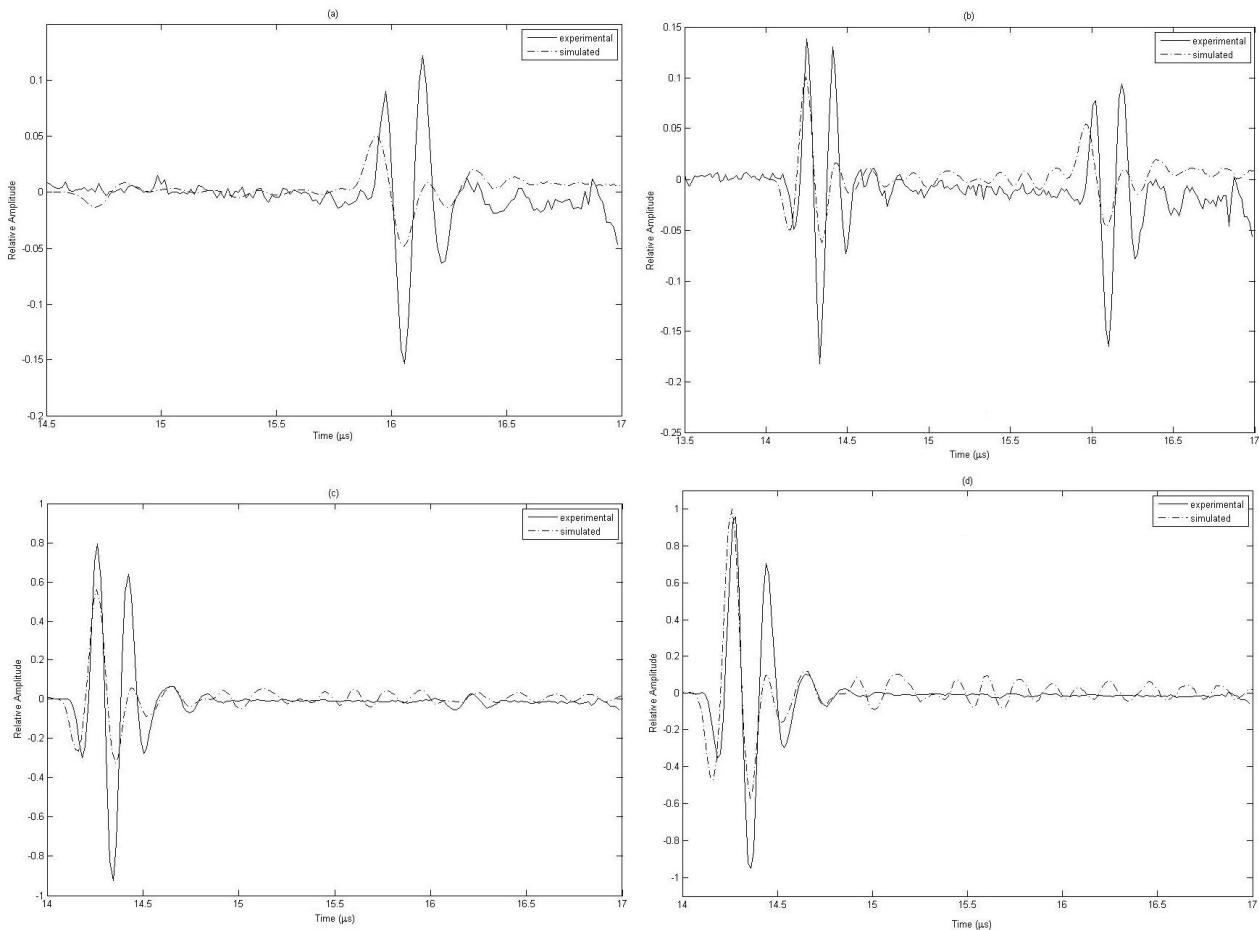
Fig.12. Discrete representation method impulse response (dash-dot line) and experimental (solid lines) signals obtained by using the 5-MHz transducer with diameter 19mm, displaced off the defect axis: (a) position 1 = 0mm, (b) position 2 = 5mm, (c) position 3 = 10mm, and (d) position 4 = 15mm.

3.1. Discretization

The discretization error is determined by two causes: first, the intrinsic error of the method, and secondly, due to the difference between the opening of the calculation resulting from the discretization and opening theory. This is reflected both in form, and the net area available for the opening discretized, which will influence the energy radiated, so that the pressure does not perform its true value [9-10].

Figure 13 shows the RMS obtained with the relation between Δx and λ, dimensionless number, the lower the Δx chosen for the discretization, the larger the computational time. The study was chosen to $\Delta x / \lambda$ of 0.3014, 0.6079, 0.6757, 0.9119, 1.2158 and 1.3514, with a frequency of 2.25 and 5MHz, with its RMS errors, respectively.

Differences in the way that can be described as visually significant are $\Delta x / \lambda > 0.61$, therefore, while values below 0.61 visual differences are much less relevant. These visual differences are presented in Figure (14), are located in certain areas.
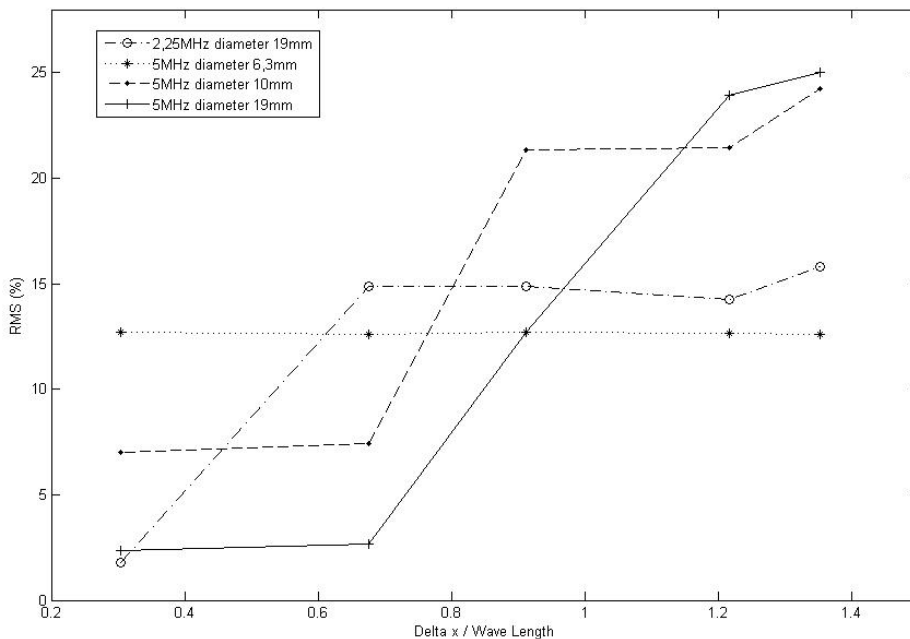
Fig. 13: Shows the profiles of $\varDelta x / \lambda$ is from 0.3014, 0.6079, 0.6757, 0.9119, 1.2158, 1.3514, for the frequency of 2.25MHz and 5MHz and their respective RMS errors.
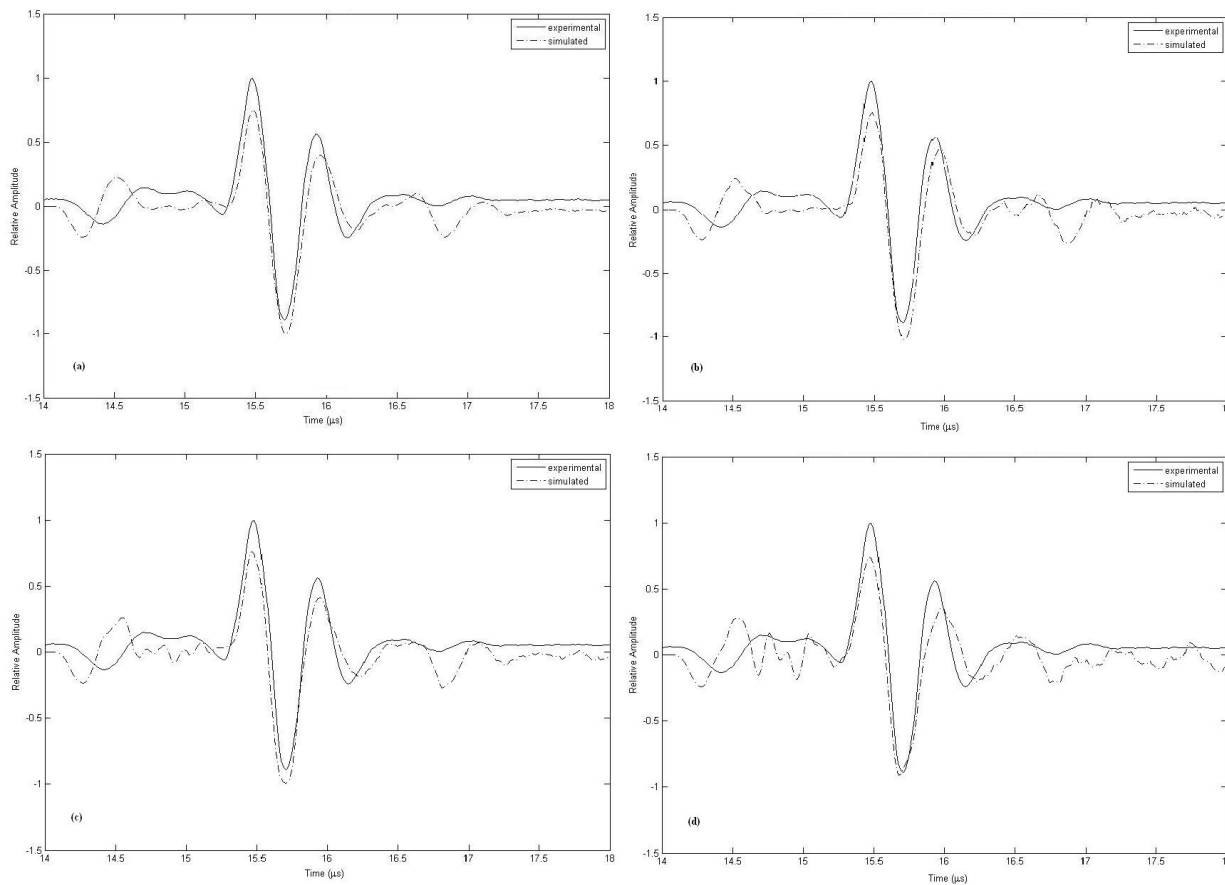

Fig.14: Discrete representation method impulse response in position 7 (dash-dot line) and experimental (solid lines) signals obtained by using the transducer of 2.25 MHz where in (a) used a $\varDelta x / \lambda$ of 0.68 in (b) a $\varDelta x / \lambda$ of 0.91 in (c) a $\varDelta x / \lambda$ of 1.22 and (d) a $\varDelta x / \lambda$ of 1.52.

Figure 14 Shows the discrete representation method impulse response and experimental in position 7 7 (dash-dot line) and experimental (solid lines) signals obtained by using the transducer of 2.25 MHz where in (a) used a $\Delta x / \lambda$ of 0.68 in (b) a $\Delta x / \lambda$ of 0.91 in (c) a $\Delta x / \lambda$ of 1.22 and (d) a $\Delta x / \lambda$ of 1.52, we find that qualitatively from $\Delta x / \lambda$ of 0.91 on the scale switch is significantly above the end of the chart, becoming even more pronounced for $\Delta x / \lambda$ of 1.52.

5. CONCLUSION

By using three 5-MHz transducers with diameters of 6.3, 10 and 19 mm and a 19mm-diam 2.25MHz transducer, and considering a Δx of 0.2mm and a slightly curved surface of the defect, a good correlation between experimental and theoretical pressure responses from a concave circular defect was shown.

The effects of defect size and position on both amplitude and shape of the echo responses were investigated. It was shown that the relative error increases as the discretization of both the transducer and the defect surface decreases. It was also shown that the smaller the diameter of the transducer, the greater will be the relative error.

The small differences among experimental and simulated waveforms are due to the difficulty to experimentally adjust the parallelism between the plane interface and the transducer. The knowledge of the pressure response simulated for a given geometry allows accurate interpretations of the echoes generated from corrosions in a realistic pipeline inspection. It provides good understanding of the spatial points where the transducers start and end traveling across the defect.

6. ACKNOWLEDGEMENTS

7. REFERENCES

Banerjee, Sourav and Kundu, Tribikram. "Semi-analytical modeling of ultrasonic fields in solids with internal anomalies immersed in a fluid", Wave Motion, Vol. 45, pp. 581–595, 2008. [10]

Belgroune, D., Belleval, J. F. de, and Djelouah H., "Theoretical study of ultrasonic wave transmission through a fluid–solid interface", Ultrasonics, vol. 48, pp. 220–230, 2008. [9]

Buiochi, F., Martínez, O., Ullate, L. G. and Espinosa, F. M. de, "A computational method to calculate the longitudinal wave evolution caused by interfaces between isotropic media", IEEE Trans. Ultrason., Ferroelect., and Freq. Contr. Vol. 51, n . 2, pp. 181-192, 2004. [3]

Harris, G. R., "Transient field of a baffled planar piston having an arbitrary vibration amplitude distribution," J. Acoust.Soc.Am.,vol.70,pp.186-204, 1981. [8]

McLaren, S., Weight, J. P., "Transmit-receive mode response from finite-sized targets in fluid media", J. Acoust. Soc. Am., vol. 82, n. 6, pp. 2102-2112, 1987. [2]

Piwakowski, B. and Delannoy, B., "Method for computing spatial pulse response: Time-domain approach", J. Acoust. Soc. Am., vol. 86, n. 6, pp. 2422-2432, 1989. [4]

Piwakowski, B. and Sbai, K., "A new approach to calculate the field radiated from arbitrarily structured transducer arrays", IEEE Trans. Ultrason., Ferroelect., and Freq. Contr., vol. 46, n. 2, pp. 422-440, 1999. [5]

Robinson, D. E., Lees, S. and Bess, L., "Near field transient radiation patterns for circular pistons," IEEE Trans. Acoust., Speech and Signal Processing, vol. 22, n. 6, pp. 395-403, 1974. [6]

Stepanishen, P. R., "Transient radiation from piston in an infinite planar baffle", J. Acoust. Soc. Am., vol. 49, pp.1629-1638, 1971. [1]

Weight, J.P., "Ultrasonic beam structures in fluid media", J. Acoust. Soc. Am., vol. 76, pp. 1184-1191, 1984. [7]